frontiers | Frontiers in Materials

TYPE Original Research
PUBLISHED 23 December 2022
DOI 10.3389/fmats.2022.1054138

Check for updates

OPEN ACCESS

EDITED BY
Ali Saleh Alshomrani,
King Abdulaziz University, Saudi Arabia

REVIEWED BY
Noreen Akbar,
National University of Sciences and Technology (NUST), Pakistan
Najeeb Alam Khan,
University of Karachi, Pakistan

*CORRESPONDENCE
Muhammad Sohail,
muhammad_sohail111@yahoo.com
Sayed M. Eldin,
sayed.eldin22@fue.edu.eg

SPECIALTY SECTION
This article was submitted to Colloidal Materials and Interfaces, a section of the journal Frontiers in Materials

RECEIVED 26 September 2022
ACCEPTED 04 November 2022
PUBLISHED 23 December 2022

CITATION
Nazir U, Sohail M, Mukdasai K, Singh A, Alahmadi RA, Galal AM and Eldin SM (2022), Applications of variable thermal properties in Carreau material with ion slip and Hall forces towards cone using a non-Fourier approach *via* FE-method and mesh-free study.
Front. Mater. 9:1054138.
doi: 10.3389/fmats.2022.1054138

COPYRIGHT
© 2022 Nazir, Sohail, Mukdasai, Singh, Alahmadi, Galal and Eldin. This is an open-access article distributed under the terms of the Creative Commons Attribution License (CC BY). The use, distribution or reproduction in other forums is permitted, provided the original author(s) and the copyright owner(s) are credited and that the original publication in this journal is cited, in accordance with accepted academic practice. No use, distribution or reproduction is permitted which does not comply with these terms.

Applications of variable thermal properties in Carreau material with ion slip and Hall forces towards cone using a non-Fourier approach *via* FE-method and mesh-free study

Umar Nazir[1], Muhammad Sohail[2]*, Kanit Mukdasai[1], Abha Singh[3], Reham A. Alahmadi[4], Ahmed M. Galal[5,6] and Sayed M. Eldin[7]*

[1]Department of Mathematics, Faculty of Science, Khon Kaen University, Khon Kaen, Thailand, [2]Department of Mathematics, Khwaja Fareed University of Engineering and Information Technology, Rahim Yar Khan, Pakistan, [3]Department of Basic Sciences, College of Sciences and Theoretical Studies, Dammam-branch, Saudi Electronic University, Riyad, Saudi Arabia, [4]Department of Basic Sciences, College of Sciences and Theoretical Studies, Medinah-branch, Saudi Electronic University, Riyad, Saudi Arabia, [5]Mechanical Engineering Department, College of Engineering, Prince Sattam Bin Abdulaziz University, Wadi addawaser, Saudi Arabia, [6]Production Engineering and Mechanical Design Department, Faculty of Engineering, Mansoura University, Mansoura, Egypt, [7]Center of Research, Faculty of Engineering, Future University in Egypt New Cairo, New Cairo, Egypt

This research highlights the utilization of two viscosity models to study the involvement of variable properties in heat and momentum transport in a rotating Carreau fluid past over a cone. The rheology of the Carreau material is assessed by the variable dynamic viscosity over the heating cone. The transport of momentum phenomenon is modeled by considering generalized Ohm's law in Carreau liquid and thermal transport in derived by considering variable thermal conductivity, heat flux model. The considered model is derived in the form of nonlinear PDEs with boundary layer analysis. The nonlinear PDEs are converted into coupled ODEs by using approximate transformation and converted equations are solved numerically by finite element methodology. The impact of numerous parameters is displayed graphically, and their behavior is discussed in detail.

KEYWORDS

finite element method, nonlinear ODEs, heat transfer, boundary layer theory, variable properties

Introduction

The features of heat transfer are applicable in several industrial, chemical, and thermal processes. This type of phenomenon is applicable in polymers, gas engineering, cooling process, solar cells, water, thermal process, and oils. Recent work on heat transfer in several rheological fluids should be mentioned. Nazeer et al. (2022) estimated the thermal aspects of multiphase flow taking into account magnetohydrodynamic and thermal radiation over a stretching frame. Luan et al. (2022) discussed turbulator effects in heat transfer phenomena in an energy transfer mechanism. Imran et al. (2022) discussed enhancement in thermal energy using the concept of several shapes of nanoparticles involving hybrid nanoparticles over a horizontal plate. The characteristics of fluids exhibit a range of rheological behavior. Therefore, it is very complex to study rheological behaviors, taking into account rheological stress (strain relation). The Newtonian model contains only viscosity rheology and its utilization in non-Newtonian contexts provides inaccurate information with respect to mass diffusion, flow, and heat energy. Carreau fluid is type of non-Newtonian fluid. Mathematical model related to Carreau fluid was investigated by Carreau (1972). The stress tensor regarding Carreau fluid is defined as

$$\boldsymbol{\tau} = -pI + \mu_0 \left[1 + \Gamma^2 \Upsilon^2\right]^{n-1/2} \boldsymbol{A}_{1.} \quad (1)$$

where $\boldsymbol{\tau}$ is the stress tensor, n is the power law index number, I is the identity matrix, A_1 is the Rivlin Ericksen tensor, and Υ^2 is the strain rate tensor. Nazir et al. (2021) discussed the rheology equations of a Carreau liquid using the impacts of ion slip and Hall forces in a rotating cone. They used a numerical approach to find numerical consequences. Sohail et al. (2022) studied three kinds of mass species in Carreau liquid in the presence of activation energy over a stretching plate. Nabwey et al. (2022) investigated the thermal aspects of Carreau nanofluid taking into account the chemical species and bioconvection in a cylinder. Reedy et al. (2022) discussed a model for a Carreau fluid including entropy generation over a heated microchannel. This involved multiple impacts based on thermal radiation and viscous dissipation using no-slip conditions. Imran et al. (2021) estimated the features of a Carreau liquid in energy transfer using magnetic dipoles and radiation containing nanofluids and microorganisms past a wedge, numerically solved with the shooting approach. Song et al. (2022) discussed thermal aspects in Carreau fluid considering nanoparticles in a stretching cylinder using Marangoni boundary conditions (BCs). Farooq et al. (2021) used Cattaneo-Christov theory in energy equations, taking thermal radiation, bioconvection flow, and heat source into account.

Recent investigations have shown that mass diffusion and thermal conductivity during transport mass species and heat cannot increase and remain constant. During changes of thermal energy, viscosity and thermal conductivity are functions of heat energy during the transport of particles. Alhussain and Tassaddiq (2022) proposed a model of variable viscosity in the presence of hybrid nanomaterial in Casson fluid, considering thin film considering magnetic field in channel. They have utilized analytical approach to simulate numerical consequences. Kumawat et al. (2022) performed numerical results of entropy generation in MHD flow considering variable viscosity in the presence of variable viscosity. Nazir et al. (2020) simulated the numerical study of a Carreau liquid using the concept of variable properties in mass diffusion and heat energy involving non-Fourier's law over a frame using finite element scheme. It was found that the highest heat energy was obtained for variable viscosity than for constant viscosity. Chaurasiya et al. (2022) discussed the influence of variable thermal conductivity taking into account semi-conductor sources using a finite element scheme. Wang et al. (2022) investigated the impacts of tri-hybridized nanofluid taking into account variable properties of fluid in the presence of non-Fourier's law computed by the FE-method. Naseem et al. (2021) discussed the numerical consequences of Soret and Dufour effects involving the role of thermal radiation over a stretching frame, including variable thermal conductivity. Sohail et al. (2021) investigated the performance of entropy generation in a Casson fluid inserting the impact of Lorentz force. They discussed features of variable properties including various effects past a stretching frame. Akbar et al. (2022) performed investigations of unsteady flow in peristaltic transport using variable viscosity (function of temperature) simulating an exact solution approach. Akram et al. (2022a) estimated the thermal features of peristaltic flow involving electroosmotically adding a suspension of nanomaterial in a curved microchannel. Maraj et al. (2022) developed mathematically modeling of rotational MHD flow in the presence of Hall force inserting two types of nanoparticles using slip conditions in a vertical channel. Habib and Akbar (2021) investigated a new to nanofluids using sensitive *Staphlococcus aureus* and *Staphlococcus aureus*. They concluded that drug resistance can be reduced and overcome using drug conjugate and gold nanoparticles. Akram et al. (2021) introduced thermal transfer characterizations inserting hybrid nanofluid (Ag–Au) considering electroosmotic pumping in microchannel. Akram et al. (2022b) analyzed electroosmotic flow based on water-silver nanofluids considering peristalsis flow using two various approaches of nanofluid. Akram et al. (2022c) introduced investigation of electroosmosis in the presence of MHD peristaltic flow containing suspension of SWCNTs nanofluid filled in aqueous media. Multiple aspects of Carreau liquid applied to a magnetic field in a suspension of a nanofluid using slip effects across a slandering surface were studied by Raju et al. (2019). Khan and Sultan (2015) discussed thermal features of Dufour and Soret effects in Eyring-Powell liquid using a porous heated cone. Dawar et al. (2021) investigated flow configurations in Williamson fluid, taking into account non-

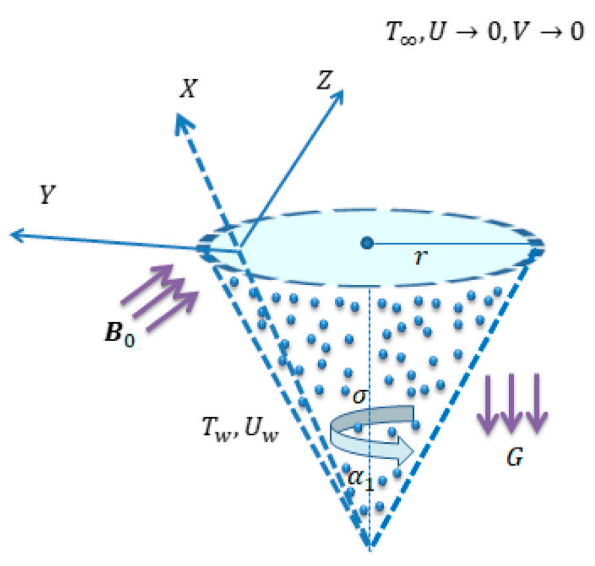

FIGURE 1
Rotating cone and coordinates system.

isosolutal conditions inserting nanofluid over wedge and cone.

The utilization of variable properties to study momentum and thermal transport in Carreau model past over a cone has not been sufficiently thoroughly studied. This contribution covers this question, and the modeled equations are solved numerically *via* finite element approach, and the impact of different involved parameters on velocity and temperature is discussed.

Mathematically development and physical consequences

zThree-dimensional thermal features in terms of variable properties in a Carreau liquid in rotating cone are visualized. Two kinds of forces, namely, ion slip and Hall forces, are considered. The rheology of a Carreau liquid in the presence of variable viscosity is imposed into fluidic motion. Heat energy assessed using the non-Fourier approach. Lorentz force is inserted along the z-direction of a heated cone. Additionally, motion associated with particles is generated due to rotational movement of cone with angle Ω. The wall temperature is considered T_w. Thermal conductivity related fluid is considered function of temperature. The rotating cone is captured by Figure 1. Boundary layer approximation (BLA) is utilized to develop model of PDEs. The reduced form of PDEs is given below. Gravitational acceleration acts downward in a cone. Figure 1 predicts the physical behavior of the model (Khan et al., 2014).

Conservation laws (Khan et al., 2014; Malik et al., 2016) are defined as follows:

$$\nabla \cdot \tilde{\boldsymbol{V}} = \boldsymbol{0}, \tag{2}$$

$$\rho_{Thnf}\left(\frac{\boldsymbol{d}\tilde{\boldsymbol{V}}}{\boldsymbol{dt}}\right) = -\nabla p + \nabla \cdot \boldsymbol{\tau} + \mathbf{J} \times \mathbf{B}, \tag{3}$$

$$\nabla \cdot \boldsymbol{B} = \boldsymbol{0}, \mu_{Thnf}\boldsymbol{J} = \nabla\times \mathbf{B}, \ , \nabla\times \mathbf{E} = \frac{\partial \boldsymbol{B}}{\partial t}, \tag{4}$$

$$\boldsymbol{J} = \left[\boldsymbol{E} + \tilde{\boldsymbol{V}}\times \mathbf{B}\right]\boldsymbol{\sigma}_{\boldsymbol{Thnf}} - (\boldsymbol{J}\times\boldsymbol{B})\frac{B_e}{|\boldsymbol{B}|} + (\boldsymbol{J}\times\boldsymbol{B})\frac{B_iB_e}{|\boldsymbol{B}|^2}\times \boldsymbol{B}, \tag{5}$$

$$\left(\rho C_p\right)_{thnf}\left(\frac{\boldsymbol{dT}}{\boldsymbol{dt}}\right) = K_{Thnf}\left(\nabla^2 T\right) - \nabla\cdot\boldsymbol{q} + Q_0\left(T - T_\infty\right). \tag{6}$$

The reduced form of the PD equations (Khan et al., 2014; Malik et al., 2016) is given below:

$$\frac{\partial(XU)}{\partial Y} + \frac{\partial(XV)}{\partial Z} = 0, \tag{7}$$

$$\begin{aligned} U\frac{\partial U}{\partial X} + W\frac{\partial U}{\partial Z} = {} & \frac{(B_0)^2\sigma}{\rho\left[(1+B_eB_i)^2 + (B_e)^2\right]}\left[VB_e - (1+B_iB_e)U\right], \\ & + \frac{V^2}{X} + G\beta(T - T_\infty)\cos\alpha \\ & + \frac{\partial}{\partial z}\left[\left\{1 + \Gamma^2\left(\frac{\partial U}{\partial y}\right)^2\right\}^{n-1/2}\frac{\partial U}{\partial z}\right], \end{aligned} \tag{8}$$

$$\begin{aligned} U\frac{\partial V}{\partial X} + W\frac{\partial V}{\partial Z} = {} & -\frac{(B_0)^2\sigma}{\rho\left[(1+B_eB_i)^2 + (B_e)^2\right]}\left[UB_e + (1+B_iB_e)V\right], \\ & -\frac{UV}{X} + \frac{\partial}{\partial z}\left[\left\{1 + \Gamma^2\left(\frac{\partial V}{\partial y}\right)^2\right\}^{n-1/2}\frac{\partial V}{\partial z}\right], \end{aligned} \tag{9}$$

$$\begin{aligned} U\frac{\partial T}{\partial X} + W\frac{\partial T}{\partial Z} = {} & \frac{1}{\rho C_p}\frac{\partial}{\partial Z}\left(K(T)\frac{\partial T}{\partial Z}\right) + \frac{Q_0}{\rho C_p}(T - T_\infty) \\ & -\frac{\lambda Q_0}{\rho C_p}\left(U\frac{\partial T}{\partial X} + W\frac{\partial T}{\partial Z}\right) \\ & -\lambda\left(U^2\frac{\partial^2 T}{\partial X^2} + W^2\frac{\partial^2 T}{\partial Z^2} + 2UW\frac{\partial^2 T}{\partial X\partial Z}\right) \\ & -\lambda\left(U\frac{\partial V}{\partial X} + W\frac{\partial V}{\partial Z}\right)\frac{\partial T}{\partial Z} \\ & -\lambda\left(U\frac{\partial U}{\partial X} + W\frac{\partial U}{\partial Z}\right)\frac{\partial T}{\partial X}. \end{aligned} \tag{10}$$

BCs (boundary conditions) (Malik et al., 2016) are

$$U = 0,\ V = \Omega X\sin\alpha,\ T = T_W,\ U \to 0,\ V \to 0, T \to T_\infty \tag{11}$$

Viscosity and thermal conductivity (Nazir et al., 2020) are functions of heat energy, as follows:

$$\begin{aligned} \frac{\mu_\infty}{\mu} &= \left[1 - \gamma(T_\infty - T)\right], \\ \frac{K(T)}{k_\infty} &= \left[1 - \epsilon\left(\frac{T_\infty - T}{T_w - T_\infty}\right)\right] \end{aligned} \tag{12}$$

The similarity variables (Malik et al., 2016) of current the analysis are

$$U = -\frac{\Omega X \sin\alpha F'}{2},\ V = \Omega X \sin\alpha G,\ W = \left(\Omega\nu_f \sin\alpha\right)^{1/2} F,$$
$$\Theta = \frac{T - T_\infty}{T_w - T_\infty}, \eta = \left(\frac{\Omega \sin\alpha}{\nu_f}\right)^{1/2} Z \tag{13}$$

Eq. 12 is known as a transformation, and the selection of the transformation is adopted to satisfy the continuity equation. Transformations are used in Eqs. 7–9. The ODEs are derived as

$$\frac{\Theta_\gamma}{\Theta_\gamma - 1}\left\{1 + n\left(WF''\right)^2\right\}\left\{1 + \left(WF''\right)^2\right\}^{n-3/2} F'''$$
$$+\frac{\Theta_\gamma}{\left(\Theta_\gamma - 1\right)^2}\left\{1 + \left(WF''\right)^2\right\}^{n-1/2} F''\Theta' + \frac{M^2}{(1+B_eB_i)^2 + (B_e)^2} \tag{14}$$
$$\left[(1+B_eB_i)F' + 2B_eG\right] + \left(\frac{1}{2}F'^2 - FF'' - 2G^2 - 2\lambda\Theta\right) = 0,$$
$$\frac{\Theta_\gamma}{\Theta_\gamma - 1}\left\{1 + n\left(WG'\right)^2\right\}\left\{1 + \left(WG'\right)^2\right\}^{n-3/2} G''$$
$$+\frac{\Theta_\gamma}{\left(\Theta_\gamma - 1\right)^2}\left\{1 + \left(WG'\right)^2\right\}^{n-1/2} G'\Theta' - \frac{M^2}{(1+B_eB_i)^2 + (B_e)^2} \tag{15}$$
$$\left[(1+B_eB_i)G - \frac{1}{2}B_eF'\right] + \left(GF' - F'G'\right) = 0,$$
$$(1+\epsilon\Theta)\Theta'' + \epsilon\left(\Theta'\right)^2 + Pr_\infty F\theta' + \gamma_1 Pr_\infty$$
$$\left[F^2\Theta'' - QF\Theta' + \frac{1}{2}FG'\Theta'\right] + Pr_\infty H_t\Theta = 0. \tag{16}$$

The Prandtl fluid at infinity is delivered as

$$Pr_\infty = (1+\epsilon\Theta)\left(1 - \frac{\Theta}{\Theta_\gamma}\right)Pr. \tag{17}$$

Substituting Eq. (16) into Eq. (15), we have

$$(1+\epsilon\Theta)\Theta'' + \epsilon\left(\Theta'\right)^2 + \gamma_1(1+\epsilon\Theta)\left(1 - \frac{\Theta}{\Theta_\gamma}\right)$$
$$Pr\left[F^2\Theta'' - QF\Theta' + \frac{1}{2}FG'\Theta'\right] + (1+\epsilon\Theta)\left(1 - \frac{\Theta}{\Theta_\gamma}\right)Pr\, F\Theta'$$
$$+ (1+\epsilon\Theta)\left(1 - \frac{\Theta}{\Theta_\gamma}\right)PrH_t\Theta = 0. \tag{18}$$

$\theta_\gamma = 1/\gamma(T_w - T_\infty)$ is the fluid viscosity number. The case is known as constant viscosity for $\theta_\gamma \to \infty$ and case for liquids for $\theta_\gamma = -1$.

Wall stresses (skin friction coefficients) are formulated as

$$Re^{1/2}C_F = \frac{\theta_\gamma}{\theta_\gamma - 1}\left[1 + W^2\left(F''(0)\right)^2\right]^{n-1/2} F''(0) \tag{19}$$
$$Re^{1/2}C_G = \frac{\theta_\gamma}{\theta_\gamma - 1}\left[1 + W^2\left(G'(0)\right)^2\right]^{n-1/2} G'(0) \tag{20}$$
$$Re^{-1/2}Nu = (1+\epsilon)\Theta'(0) \tag{21}$$

The heat transfer rate in terms of variable thermal conductivity is

Numerical methodology

The formulated ODEs are numerically simulated by a numerical scheme (FEM) [14, 16, and 31]. The description associated with FEM is mentioned below.

Discretization of domain

In this step, the desired ODEs are transformed into numbers of elements (300 elements). Residuals of the current problem are achieved. Eqs. 13–15 are strong forms with boundary conditions. A strong form can be converted into a weak form by collecting all terms on one side and multiplying it by weight functions and integrated it on whole domain. The weighted residuals of the problem implementation due to $F' = S$ are as follows:

$$\int_{\eta_e}^{\eta_{e+1}} w_1\left(F' - S\right)d\eta = 0, \tag{22}$$

$$\int_{\eta_e}^{\eta_{e+1}} w_2 \begin{bmatrix} \frac{\Theta_\gamma}{\Theta_\gamma - 1}\left\{1 + n\left(WF''\right)^2\right\}\left\{1 + \left(WF''\right)^2\right\}^{n-3/2} S'' \\ +\frac{M^2}{(1+B_eB_i)^2 + (B_e)^2}\left[(1+B_eB_i)F' + 2B_eG\right] \\ \left(\frac{1}{2}F'^2 - FF'' - 2G^2 - 2\lambda\Theta\right) \end{bmatrix} d\eta = 0, \tag{23}$$

$$\int_{\eta_e}^{\eta_{e+1}} w_3 \begin{bmatrix} \frac{\Theta_\gamma}{\Theta_\gamma - 1}\left\{1 + n\left(WG'\right)^2\right\}\left\{1 + \left(WG'\right)^2\right\}^{n-3/2} G'' \\ +\frac{\Theta_\gamma}{\left(\Theta_\gamma - 1\right)^2}\left\{1 + \left(WG'\right)^2\right\}^{n-1/2} G'\Theta' + \left(GF' - F'G'\right) \\ -\frac{M^2}{(1+B_eB_i)^2 + (B_e)^2}\left[(1+B_eB_i)G - \frac{1}{2}B_eF'\right] \end{bmatrix} d\eta = 0, \tag{24}$$

$$\int_{\eta_e}^{\eta_{e+1}} w_4 \begin{bmatrix} +(1+\epsilon\Theta)\left(1 - \frac{\Theta}{\Theta_\gamma}\right)Pr\, F\Theta' + (1+\epsilon\Theta)\left(1 - \frac{\Theta}{\Theta_\gamma}\right)PrH_t\Theta \\ \gamma_1(1+\epsilon\Theta)\left(1 - \frac{\Theta}{\Theta_\gamma}\right)Pr\left[F^2\Theta'' - QF\Theta' + \frac{1}{2}FG'\Theta'\right] \\ (1+\epsilon\Theta)\Theta'' + \epsilon\left(\Theta'\right)^2 \end{bmatrix} d\eta$$
$$= 0, \tag{25}$$

Shape functions

Various shape functions are utilized in the current problem. In this approach, however, a linear shape function is implemented to obtain an approximate solution. Several shape functions are used in FEM. However, the linear type of shape function is utilized in this numerical approach. Shape functions are based on a linear type of polynomial. The values variables (N, F, Θ) are defined as

$$N = \sum_{j=1}^{2}\left(N_j\psi_j\right),\ F = \sum_{j=1}^{2}\left(F_j\psi_j\right),\ \Theta = \sum_{j=1}^{2}\left(\Theta_j\psi_j\right). \tag{26}$$

Shape functions are

$$\psi_j = (-1)^{j-1}\frac{\eta-\eta_{j-1}}{\eta_j-\eta_{j-1}}. \tag{27}$$

Developments of stiffness matrices using assemble process

The Galerkin approach is utilized to derive the stiffness matrices. The concept of the assembly process is implemented to find stiffness matrices and global stiffness matrix. The sizes of the boundary vectors, stiffness matrices, and source vectors are

$$K_{ij}^{11} = \int_{\eta_e}^{\eta_{e+1}}\left(\frac{d\psi_j}{d\eta}\psi_i\right)d\eta,\ K_{ij}^{12} = \int_{\eta_e}^{\eta_{e+1}}\left(\psi_j\psi_i\right)d\eta,\ b_i^1 = 0, K_{ij}^{13} = 0,\ K_{ij}^{14} = 0, \tag{28}$$

$$K_{ij}^{22} = \int_{\eta_e}^{\eta_{e+1}}\left[\begin{array}{c} -\dfrac{\Theta_\gamma}{\Theta_\gamma-1}\left\{1+n\left(W\bar{S}'\right)^2\right\}\left\{1+\left(W\bar{S}'\right)^2\right\}^{n-3/2}\dfrac{d\psi_i}{d\eta}\dfrac{d\psi_j}{d\eta} \\ \dfrac{\Theta_\gamma}{\left(\Theta_\gamma-1\right)^2}\left\{1+\left(WF''\right)^2\right\}^{n-1/2}\bar{\Theta}'\psi_i\dfrac{d\psi_j}{d\eta}+\dfrac{1}{2}\bar{S}\psi_i\psi_j \\ -\bar{F}\psi_i\dfrac{d\psi_j}{d\eta}+\dfrac{M^2\left(1+B_eB_i\right)}{\left(1+B_eB_i\right)^2+\left(B_e\right)^2}\psi_i\psi_j \end{array}\right] d\eta,\ b_i^2 = 0, K_{ij}^{21} = 0, \tag{29}$$

$$K_{ij}^{23} = \int_{\eta_e}^{\eta_{e+1}}\left[\frac{M^2 2B_e}{\left(1+B_eB_i\right)^2+\left(B_e\right)^2}\psi_i\psi_j - 2\bar{G}\psi_i\psi_j\right]d\eta,\ K_{ij}^{24} = \int_{\eta_e}^{\eta_{e+1}}\left[-2\lambda\bar{G}\psi_i\psi_j\right]d\eta, \tag{30}$$

$$K_{ij}^{33} = \int_{\eta_e}^{\eta_{e+1}}\left[\begin{array}{c} -\dfrac{\Theta_\gamma}{\Theta_\gamma-1}\left\{1+n\left(WG'\right)^2\right\}\left\{1+\left(WG'\right)^2\right\}^{n-3/2}\dfrac{d\psi_i}{d\eta}\dfrac{d\psi_j}{d\eta} \\ \dfrac{\Theta_\gamma}{\left(\Theta_\gamma-1\right)^2}\left\{1+\left(WG'\right)^2\right\}^{n-1/2}\bar{\Theta}'\psi_i\dfrac{d\psi_j}{d\eta}+\bar{G}\psi_i\psi_j+H\psi_i\dfrac{d\psi_j}{d\eta} \\ -\dfrac{M^2\left(1+B_eB_i\right)}{\left(1+B_eB_i\right)^2+\left(B_e\right)^2}\psi_i\psi_j \end{array}\right]d\eta, \tag{31}$$

$$K_{ij}^{32} = \int_{\eta_e}^{\eta_{e+1}}\left[\frac{M^2 1/2}{\left(1+B_eB_i\right)^2+\left(B_e\right)^2}\psi_i\psi_j\right]d\eta, K_{ij}^{34} = 0,\ K_{ij}^{31} = 0,\ b_i^3 = 0, \tag{32}$$

$$K_{ij}^{44} = \int_{\eta_e}^{\eta_{e+1}}\left[\begin{array}{c} -\left(1+\epsilon\bar{\Theta}\right)\dfrac{d\psi_i}{d\eta}\dfrac{d\psi_j}{d\eta}+\epsilon\bar{\Theta}\psi_i\dfrac{d\psi_j}{d\eta} \\ +\left(1+\epsilon\bar{\Theta}\right)\left(1-\dfrac{\bar{\Theta}}{\Theta_\gamma}\right)Pr\left(1-\dfrac{\bar{\Theta}}{\Theta_\gamma}\right)\bar{F}\psi_i\dfrac{d\psi_j}{d\eta} \\ +\left(1+\epsilon\bar{\Theta}\right)\left(1-\dfrac{\bar{\Theta}}{\Theta_\gamma}\right)PrH_t\psi_i\psi_j \\ +\gamma_1\left(1+\epsilon\bar{\Theta}\right)\left(1-\dfrac{\bar{\Theta}}{\Theta_\gamma}\right)Pr\left[\bar{F}^2\dfrac{d\psi_j}{d\eta}\dfrac{d\psi_j}{d\eta}-Q\bar{F}\Theta'+\dfrac{1}{2}\bar{F}G'\psi_i\dfrac{d\psi_j}{d\eta}\right] \end{array}\right]d\eta, \tag{33}$$

$$K_{ij}^{41} = 0,\ b_i^4 = 0,\ K_{ij}^{42} = 0,\ K_{ij}^{43} = 0. \tag{34}$$

Assembly method

The assembly method is used to assemble all elements. The residual is defined as

$$[R] = \left[M\left(F^{(r-1)}, S^{(r-1)}, \Theta^{(r-1)}, \phi^{(r-1)}\right)\right]\begin{bmatrix} F^r \\ G^r \\ S^r \\ \Theta^r \end{bmatrix} = [F]. \tag{35}$$

The convergence of the problem must existed under 10^{-5}, which is delivered as

$$\frac{\left(\sum_{i=1}^{N}\left(|\omega^r-\omega^{r-1}|\right)^2\right)^{1/2}}{\left(\sum_{i=1}^{N}|\omega^r|\right)^2} < 10^{-5}. \tag{36}$$

Code development and validation

Code based on FEM is developed on MAPLE. The Galerkin finite element method is used to simulate the problem on MAPLE 18. The FEM code is verified in a published study (Malik et al., 2016), which is recorded in Table 1. The grid-independent analysis is shown in Table 2.

Outcomes and discussion

The three-dimensional thermal aspects of a Carreau liquid in the presence of variable viscosity in a rotating cone are developed. Features related to ion slip and Hall theory are added in momentum equations. The concept associated with Cattaneo-Christov model (CCM) is utilized, involving heat generation/heat absorption. Moreover, variable fluidic properties are utilized in terms of variable thermal conductivity and viscosity dependent

TABLE 1 Validation of results in term of shear stresses and Nusselt number when $H_s = 0.0$, $Pr = 0.7$, $Ec = 0.0$, $\beta_e = 0.0$, $\beta_i = 0.0$, and $\beta = 0.2$.

	Present work			Malik et al. (2016)		
λ	$-(Re)^{1/2}C_f$	$-(Re)^{1/2}C_g$	$-(Re)^{-1/2}NU$	$-(Re)^{1/2}C_f$	$-(Re)^{1/2}C_g$	$-(Re)^{-1/2}NU$
0.0	1.0253652070	0.61537912903	0.4294230670	1.0253	0.6153	0.4295
1.0	2.20070023051	0.844695060970	0.6121076213	2.2007	0.8492	0.6121
10	8.5043340330	1.39961520634	1.0098376217	8.5041	1.3990	1.0097

TABLE 2 Grid-independent investigation for $G(\eta_{\max}/2)$, $\Theta(\eta_{\max}/2)$, and $F'(\eta_{\max}/2)$.

e	$F'(\eta_{\max}/2)$	$G(\eta_{\max}/2)$	$\Theta(\eta_{\max}/2)$
20	0.6192543746	0.7775868422	0.02364363915
40	0.3563679813	0.6172517630	0.008213654544
60	0.3472652177	0.6085798291	0.008467428871
80	0.3426854561	0.6042412374	0.008565535885
100	0.3399304701	0.6016370351	0.008615382875
120	0.3380909312	0.5999004990	0.008644849238
140	0.3367764901	0.5986602893	0.008664143487
180	0.3350215280	0.5970053059	0.008687496783
200	0.3344073091	0.5964262953	0.008695060976
220	0.3339043627	0.5959524702	0.008700980450
240	0.5955576215	0.5955576215	0.008705785061
260	0.3331306142	0.5952230675	0.008709730703
280	0.3339886777	0.5951914530	0.004266023555
300	0.3325627516	0.5951883042	0.004215755900

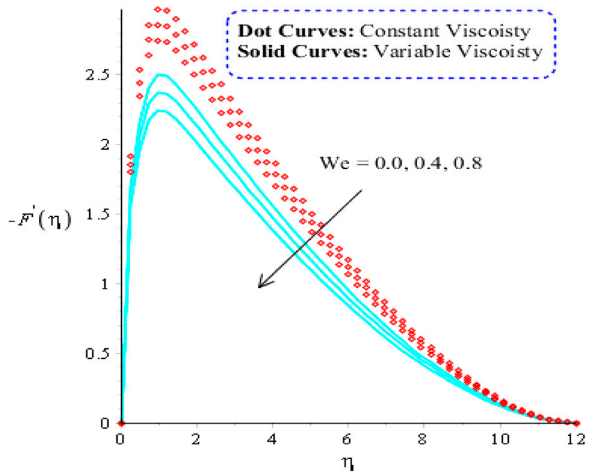

FIGURE 2
Variation in primary velocity field versus We.

heat energy. The developed model is numerically solved using the finite element approach. The graphical results in view of thermal and velocity field are shown below.

Contrast among constant and variable viscosities in velocity field

In this section, Figures 2–9 are plotted reading secondary and primary velocity fields against several parameters. It is noted that dot curves are associated with constant viscosity for $1/\Theta_\gamma = 0$, and solid curves are plotted for representation of variable viscosity for $\Theta_\gamma = -1$. Figures 2, 3 are plotted to notice variation in secondary and $G(\eta)$ velocities against change in We. The flow associated with secondary and primary velocity curves slows down against change in We. The flow for the case of constant viscosity is higher than the flow for variable viscosity. Thickness of the momentum layer is decreased when We is inclined. Physically, We is known as the Weissenberg parameter, and it is defined as the ratio between elastic force and viscous force. From definition point of view, We is inversely proportional against viscous force. Therefore, the viscosity of fluidic particles is enhanced when We is increased. Figures 4–7 are plotted to determine the visualization of velocities in the presence of ion slip and Hall parameters. For this case, flow of Carreau liquid is enhanced when ion slip and Hall numbers are increased. This is because generalized Ohm's theory is utilized in current analysis. Moreover, the directly proportional relation is predicted among ion slip and Hall parameters. Lorentz force is visualized against implication of B_e and B_i. Therefore, Lorentz force is decreased when B_e and B_i are increased. Lorentz force is produced using a generalized Ohm's law in momentum equations. The production of electron frequency and electron collision (time) is known as B_e. In additionally, the production of ion cyclotron frequency and ion collision time is called B_i. Fluidic velocity is enhanced when collision and frequency among particles are enhanced. The layers of momentum in terms of thickness is an increasing function versus the implication of B_e and B_i. Therefore, significant acceleration is produced among the particles. Thickness regarding MLs (momentum layers) for constant viscosity ($\Theta_\gamma \to \infty$) is greater than for variable viscosity. The impact of

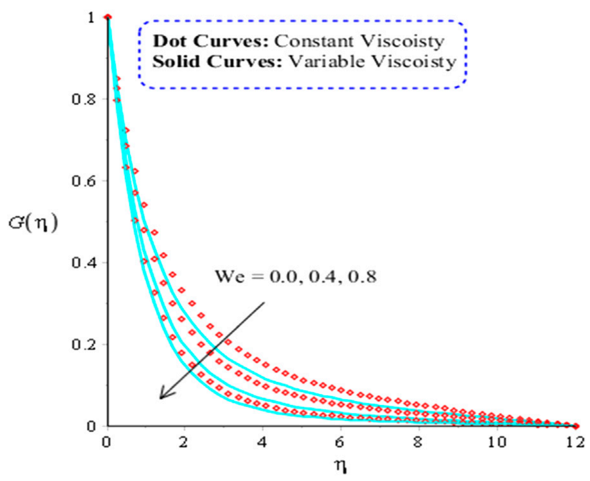

FIGURE 3
Variation in secondary velocity field versus *We*.

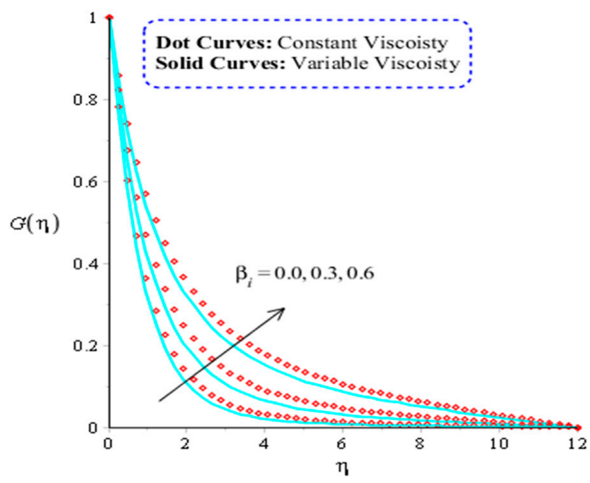

FIGURE 5
Variation in secondary velocity field versus β_i.

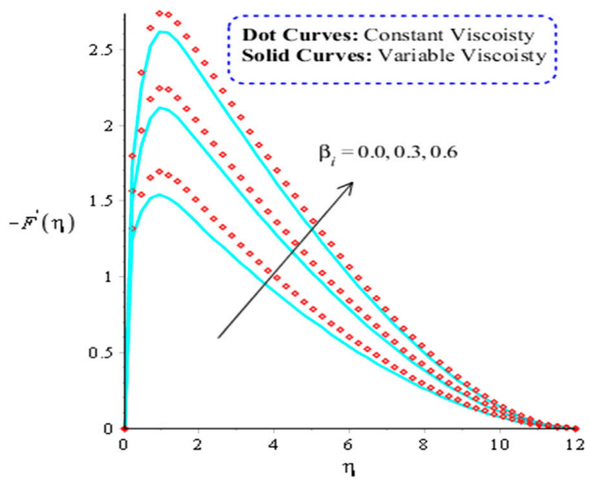

FIGURE 4
Variation in primary velocity field versus β_i.

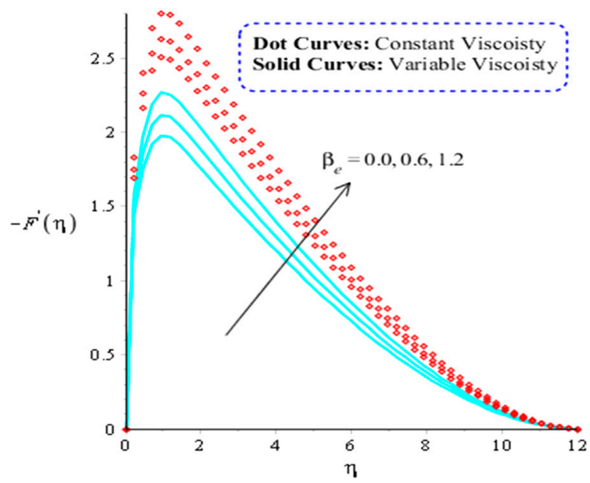

FIGURE 6
Variation in primary velocity field versus β_e.

Θ_γ on velocity fields (primary and secondary directions) is addressed by Figures 8, 9. Θ_γ is defined as $1/\gamma(T_w - T_\infty)$, while Θ_γ has inversely proportional against temperature difference. Temperature differences increase among fluidic particles. Therefore, thickness regarding momentum layers is increased versus change in Θ_γ. Mathematically, Θ_γ has directly proportional relation versus the impact of velocity fields. Therefore, flow declines when Θ_γ also decreases.

Contrast among constant and variable viscosities in temperature field

This subsection contains graphical explanation associated with thermal impacts for two cases (variable viscosity and constant viscosity) against change in heat source, ϵ, Θ_γ, and Pr. These results are shown in Figures 10–13. It is noticed that dot curves are plotted for constant viscosity ($\Theta_\gamma \to \infty$), and solid curves are

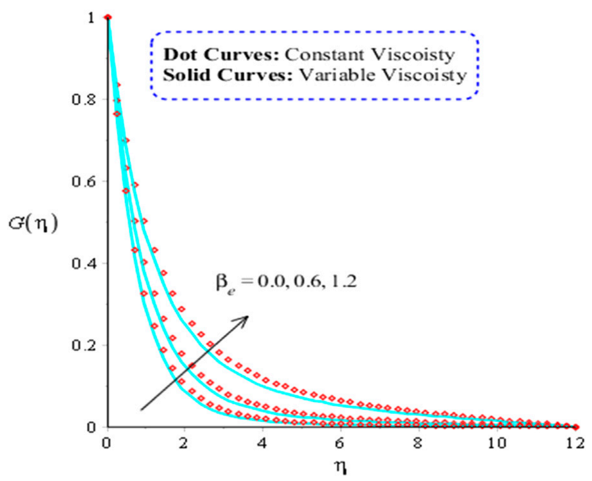

FIGURE 7
Variation in secondary velocity filed versus β_e.

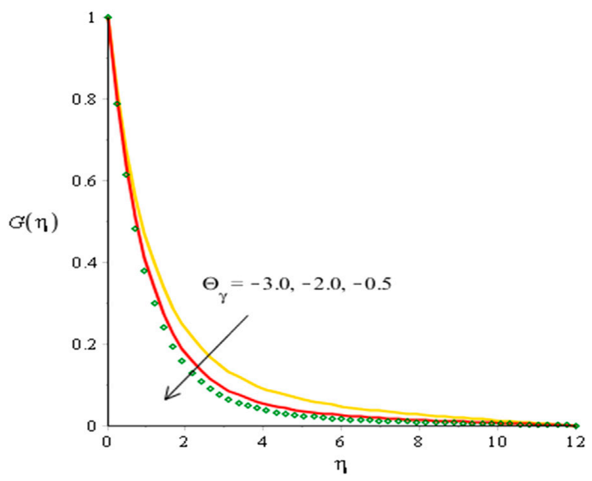

FIGURE 9
Variation in secondary velocity field versus Θ_γ.

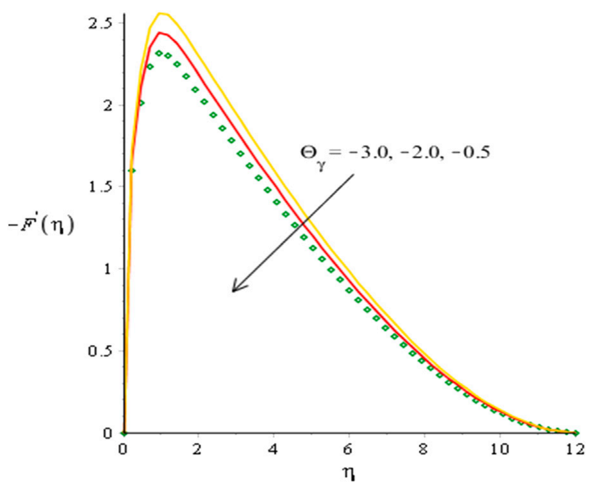

FIGURE 8
Variation in velocity field versus Θ_γ.

plotted for viscosity (function of temperature). Figure 10 is prepared to determine the impact of H_t on the thermal profile. It is addressed that heat energy is boosted when H_t is increased. Physically, this occurs due to external heat sources on the thermal profile. Hence, extra heat energy can be added using an external heat source. Additionally, heat energy for constant viscosity is greater than heat energy for case of variable viscosity. It can be noted that the behavior of H_t is based on numerical values. For negative values, H_t is called heat absorption while H_t is called heat absorption for positive values. An effect for $H_t > 0$ on temperature performance is greater than effect for $H_t < 0$. Thermal layers thickness can be adjusted trough variation in H_t whereas H_t is directly proportional against temperature difference. Therefore, heat energy is significantly increased when H_t is enhanced. The role of Pr on thermal profile is addressed in Figure 11. Thermal profile decreases against change in Pr . Physically, it refers to division among thermal thickness and momentum thickness. It is observed that inverse proportional relation is experienced between Pr and thermal layers. Consequently, thickness for thermal layers is significantly enhanced when Pr is increased. Therefore, heat energy and TBL (thermal boundary layer) can be controlled using numerical values of Pr . Figure 12 captures the impact of ϵ on thermal profile. Mathematically, a directly proportional relationship can be seen among ϵ and temperature difference. Consequently, heat energy is boosted when ϵ is increased. Figure 13 is based on the relationship between heat energy and Θ_γ. ϵ is dimensionless parameter, which is appeared using concept of non-uniform thermal conductivity. ϵ is appeared in Eq. 11, which has direct proportional relation against temperature dependence (thermal conductivity). Therefore, the temperature difference among particles is increased when ϵ is increased. Physically, temperature increases among particles due to temperature differences. Thermal energy is seen against change in Θ_γ. It can be noted that thermal energy is decreased against decline values of Θ_γ. Mathematically, Θ_γ is termed as $1/\gamma(T_w - T_\infty)$, which is inversely proportional versus temperature difference $(T_w - T_\infty)$. Hence, temperature difference is decreased when Θ_γ is increased.

Measurement of shear stresses and temperature gradient

Table 3 demonstrates the impacts of shear stresses and Nusselt numbers against variation in Pr, M, H_t, and Θ_γ. From this table, it can be seen that shear stresses are declined

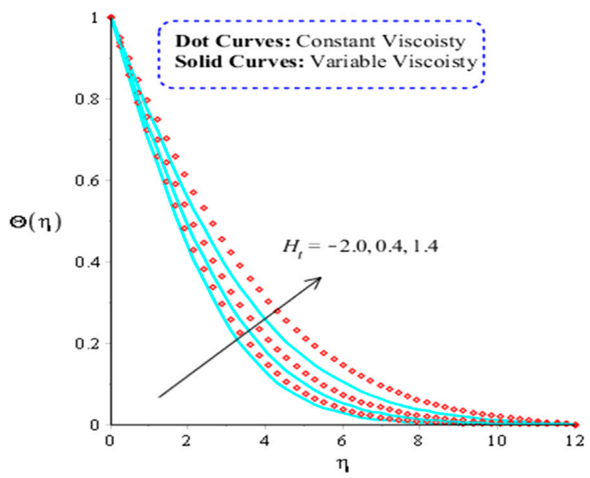

FIGURE 10
Variation in temperature field versus H_t.

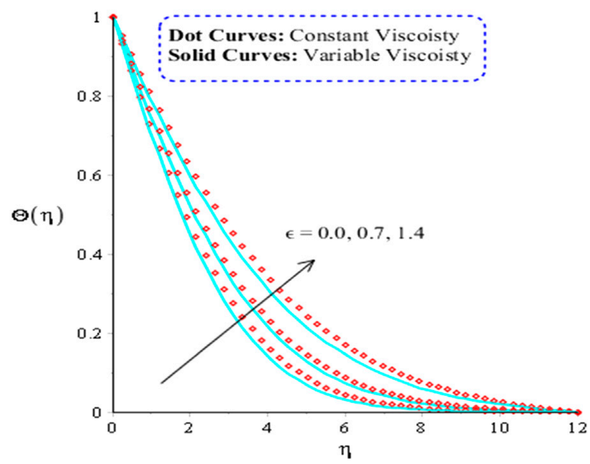

FIGURE 12
Variation in temperature field versus ϵ.

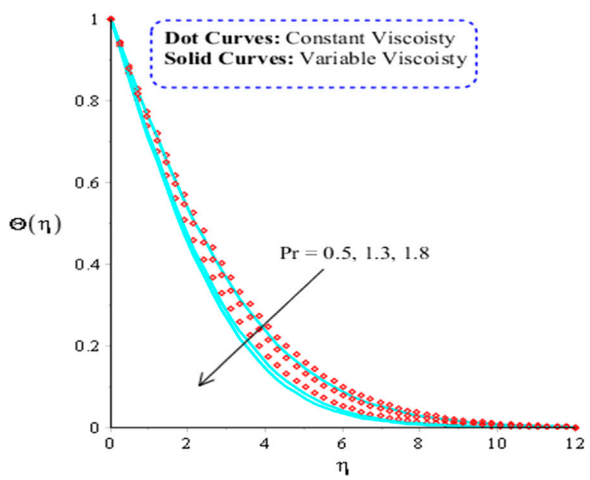

FIGURE 11
Variation in temperature field versus Pr.

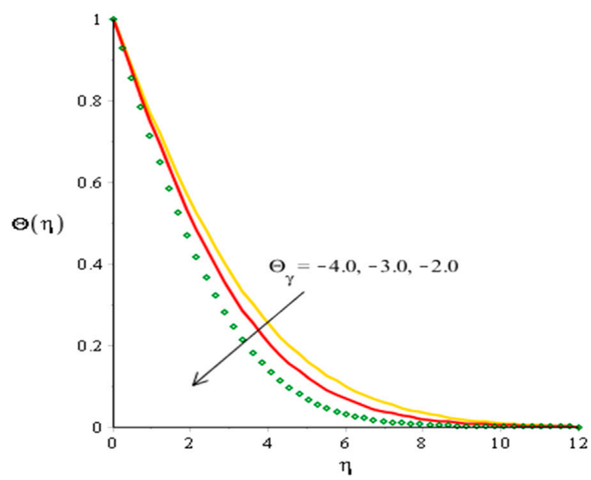

FIGURE 13
Variation in temperature field versus Θ_γ.

versus implication of H_t. However, heat transfer rate is reduced when H_t is increased. M is magnetic parameter, which is appeared using concept of Lorentz force. Divergent forces (skin friction coefficients) are decreased versus the implications of the Lorentz force. The Nusselt number (temperature gradient) is enhanced against the implications of higher-impact Lorentz forces. Velocity is increased when the Lorentz force is enhanced Shear stresses are significantly declined when the Lorentz force is enhanced. These outcomes are presented in Table 3. Additionally, the Prandtl number arguments thermal rate (Nusselt number), and shear stresses are decreased when Pr is enhanced. The division between momentum and thermal layers is represented by Pr. Therefore, skin friction coefficients are enhanced when Pr is increased.

Prime consequences of performed research

The thermal features of 3D-Carreau model are developed under considerations of ion slip and Hall forces in rotating cone. Variable thermal properties in term of viscosity, mass diffusion, and thermal conductivity are addressed. Chemical species and external heat sources are utilized in the presence of a non-Fourier law. The following are the most important outcomes from this investigation:

TABLE 3 Numerical impacts of shear stresses and temperature gradient versus Pr , M, H_t, and Θ_y.

Change in parameters		$-Re^{1/2}C_F$	$-Re^{1/2}C_G$	$-Re^{-1/2}Nu$
	0.0	0.4438288364	0.2137193533	1.337499994
Pr	0.5	0.4364839833	0.2051746254	1.224569168
	0.7	0.4200424336	0.1966019057	1.066393504
	−1.5	0.3387190600	0.08922203657	1.424510434
H_t	0.2	0.3271335238	0.02858202051	1.397533801
	0.7	0.3111766612	0.01462798772	1.373425184
	0.0	0.3740169115	0.1282122993	1.370310731
M	0.3	0.3840217314	0.1382043278	1.270316816
	0.6	0.3940361885	0.1481804049	1.170335265
	−1.5	0.3745150981	0.1274641174	1.370934176
Θ_y	−1.8	0.3848934552	0.1368848568	1.381406714
	−2.0	0.3951193643	0.1465341738	1.391688290

The computations of the problem become grid independent at 300 elements;
Heat energy diffuses faster into non-Newtonian liquids for temperature-dependent viscosity than for the diffusion of heat energy for constant viscosity;
Motion into fluidic particles is enhanced against higher values of ion slip and Hall currents parameters;
Heat energy is boosted versus higher values of H_t, but heat energy is decreased when the Prandtl number is increased;
An enhancement in thermal energy occurs according to ϵ, utilized in the production of solar energy, cooking, baking, cooling, drying, and heating;
The thermal transfer rate is applicable in metal grinding, wire paintings, glasses melting, chemical products, solar collectors, machine cutting, food processing, electronic components, nuclear reaction, solar systems, glass fiber, and so on.

Data availability statement

The raw data supporting the conclusions of this article will be made available by the authors, without undue reservation.

Author contributions

UN: Conceptualization; Investigation; Software; Validation; Writing—review and editing. MS: Data curation; Writing—original draft; Writing—review and editing; Visualization; Methodology. KM: Formal analysis; Funding acquisition; Software. AS: Methodology; Project administration; Resources; Funding acquisition. RA: Project administration; Formal analysis. AG: Visualization; Supervision; Funding acquisition. MS: Software; Validation; Visualization; Supervision; Funding acquisition.

Funding

This work was partially funded by the research center of the Future University in Egypt, 2022.

Conflict of interest

The authors declare that the research was conducted in the absence of any commercial or financial relationships that could be construed as a potential conflict of interest.

Publisher's note

All claims expressed in this article are solely those of the authors and do not necessarily represent those of their affiliated organizations, or those of the publisher, the editors, and the reviewers. Any product that may be evaluated in this article, or claim that may be made by its manufacturer, is not guaranteed or endorsed by the publisher.

References

Akbar, N. S., Maraj, E. N., Noor, N. F. M., and Habib, M. B. (2022). Exact solutions of an unsteady thermal conductive pressure driven peristaltic transport with temperature-dependent nanofluid viscosity. *Case Stud. Therm. Eng.* 35, 102124. doi:10.1016/j.csite.2022.102124

Akram, J., Akbar, N. S., Alansari, M., and Tripathi, D. (2022). Electroosmotically modulated peristaltic propulsion of TiO2/10W40 nanofluid in curved microchannel. *Int. Commun. Heat Mass Transf.* 136, 106208. doi:10.1016/j.icheatmasstransfer.2022.106208

Akram, J., Akbar, N. S., and Tripathi, D. (2021). A theoretical investigation on the heat transfer ability of water-based hybrid (Ag–Au) nanofluids and Ag nanofluids flow driven by electroosmotic pumping through a microchannel. *Arab. J. Sci. Eng.* 46 (3), 2911–2927. doi:10.1007/s13369-020-05265-0

Akram, J., Akbar, N. S., and Tripathi, D. (2022). Analysis of electroosmotic flow of silver-water nanofluid regulated by peristalsis using two different approaches for nanofluid. *J. Comput. Sci.* 62, 101696. doi:10.1016/j.jocs.2022.101696

Akram, J., Akbar, N. S., and Tripathi, D. (2022). Electroosmosis augmented MHD peristaltic transport of SWCNTs suspension in aqueous media. *J. Therm. Anal. Calorim.* 147 (3), 2509–2526. doi:10.1007/s10973-021-10562-3

Alhussain, Z. A., and Tassaddiq, A. (2022). Thin film blood based Casson hybrid nanofluid flow with variable viscosity. *Arab. J. Sci. Eng.* 47 (1), 1087–1094. doi:10.1007/s13369-021-06067-8

Carreau, P. J. (1972). Rheological equations from molecular network theories. *Trans. Soc. Rheology* 16 (1), 99–127. doi:10.1122/1.549276

Chaurasiya, V., Chaudhary, R. K., Awad, M. M., and Singh, J. (2022). A numerical study of a moving boundary problem with variable thermal conductivity and temperature-dependent moving PCM under periodic boundary condition. *Eur. Phys. J. Plus* 137 (6), 714. doi:10.1140/epjp/s13360-022-02927-w

Dawar, A., Shah, Z., Tassaddiq, A., Kumam, P., Islam, S., and Khan, W. (2021). A convective flow of Williamson nanofluid through cone and wedge with non-isothermal and non-isosolutal conditions: A revised buongiorno model. *Case Stud. Therm. Eng.* 24, 100869. doi:10.1016/j.csite.2021.100869

Farooq, U., Waqas, H., Khan, M. I., Khan, S. U., Chu, Y. M., and Kadry, S. (2021). Thermally radioactive bioconvection flow of Carreau nanofluid with modified Cattaneo-Christov expressions and exponential space-based heat source. *Alexandria Eng. J.* 60 (3), 3073–3086. doi:10.1016/j.aej.2021.01.050

Habib, M. B., and Akbar, N. S. (2021). New trends of nanofluids to combat *Staphylococcus aureus* in clinical isolates. *J. Therm. Anal. Calorim.* 143 (3), 1893–1899. doi:10.1007/s10973-020-09502-4

Imran, M., Farooq, U., Muhammad, T., Khan, S. U., and Waqas, H. (2021). Bioconvection transport of Carreau nanofluid with magnetic dipole and nonlinear thermal radiation. *Case Stud. Therm. Eng.* 26, 101129. doi:10.1016/j.csite.2021.101129

Imran, M., Yasmin, S., Waqas, H., Khan, S. A., Muhammad, T., Alshammari, N., et al. (2022). Computational analysis of nanoparticle shapes on hybrid nanofluid flow due to flat horizontal plate via solar collector. *Nanomaterials* 12 (4), 663. doi:10.3390/nano12040663

Khan, N. A., Aziz, S., and Khan, N. A. (2014). Numerical simulation for the unsteady MHD flow and heat transfer of couple stress fluid over a rotating disk. *PLoS One* 9 (5), e95423. doi:10.1371/journal.pone.0095423

Khan, N. A., and Sultan, F. (2015). On the double diffusive convection flow of Eyring-Powell fluid due to cone through a porous medium with Soret and Dufour effects. *AIP Adv.* 5 (5), 057140. doi:10.1063/1.4921488

Kumawat, C., Sharma, B. K., Al-Mdallal, Q. M., and Rahimi-Gorji, M. (2022). Entropy generation for MHD two phase blood flow through a curved permeable artery having variable viscosity with heat and mass transfer. *Int. Commun. Heat Mass Transf.* 133, 105954. doi:10.1016/j.icheatmasstransfer.2022.105954

Luan, X. D., Xu, Y. P., Ayed, H., and Selim, M. M. (2022). Heat transfer treatment of nanomaterial with considering turbulator effects. *Int. Commun. Heat Mass Transf.* 131, 105787. doi:10.1016/j.icheatmasstransfer.2021.105787

Malik, M. Y., Jamil, H., Salahuddin, T., Bilal, S., Rehman, K. U., and Mustafa, Z. (2016). Mixed convection dissipative viscous fluid flow over a rotating cone by way of variable viscosity and thermal conductivity. *Results Phys.* 6, 1126–1135. doi:10.1016/j.rinp.2016.11.027

Maraj, E. N., Zehra, I., and SherAkbar, N. (2022). Rotatory flow of MHD (MoS2-SiO2)/H2O hybrid nanofluid in a vertical channel owing to velocity slip and thermal periodic conditions. *Colloids Surfaces A Physicochem. Eng. Aspects* 639, 128383. doi:10.1016/j.colsurfa.2022.128383

Nabwey, H. A., Alshber, S. I., Rashad, A. M., and Mahdy, A. E. N. (2022). Influence of bioconvection and chemical reaction on magneto-Carreau nanofluid flow through an inclined cylinder. *Mathematics* 10 (3), 504. doi:10.3390/math10030504

Naseem, T., Nazir, U., El-Zahar, E. R., Algelany, A. M., and Sohail, M. (2021). Numerical computation of Dufour and Soret effects on radiated material on a porous stretching surface with temperature-dependent thermal conductivity. *Fluids* 6 (6), 196. doi:10.3390/fluids6060196

Nazeer, M., Saleem, S., Hussain, F., Zia, Z., Khalid, K., and Feroz, N. (2022). Heat transmission in a magnetohydrodynamic multiphase flow induced by metachronal propulsion through porous media with thermal radiation. *Proc. Institution Mech. Eng. Part E J. Process Mech. Eng.*, 095440892210752. doi:10.1177/09544089221075299

Nazir, U., Saleem, S., Nawaz, M., Sadiq, M. A., and Alderremy, A. A. (2020). Study of transport phenomenon in Carreau fluid using Cattaneo–Christov heat flux model with temperature dependent diffusion coefficients. *Phys. A Stat. Mech. its Appl.* 554, 123921. doi:10.1016/j.physa.2019.123921

Nazir, U., Sohail, M., Selim, M. M., Alrabaiah, H., and Kumam, P. (2021). Finite element simulations of hybrid nano-Carreau Yasuda fluid with hall and ion slip forces over rotating heated porous cone. *Sci. Rep.* 11 (1), 19604–19615. doi:10.1038/s41598-021-99116-z

Raju, C. S. K., Hoque, M. M., Khan, N. A., Islam, M., and Kumar, S. (2019). Multiple slip effects on magnetic-Carreau fluid in a suspension of gyrotactic microorganisms over a slendering sheet. *Proc. Institution Mech. Eng. Part E J. Process Mech. Eng.* 233 (2), 254–266. doi:10.1177/0954408918776723

Reedy, S., Srihari, P., Ali, F., and Naikoti, K. (2022). Numerical analysis of Carreau fluid flow over a vertical porous microchannel with entropy generation. *Partial Differ. Equations Appl. Math.* 5, 100304. doi:10.1016/j.padiff.2022.100304

Sohail, M., Chu, Y. M., El-Zahar, E. R., Nazir, U., and Naseem, T. (2021). Contribution of joule heating and viscous dissipation on three dimensional flow of Casson model comprising temperature dependent conductance utilizing shooting method. *Phys. Scr.* 96 (8), 085208. doi:10.1088/1402-4896/ac00e5

Sohail, M., Nazir, U., El-Zahar, E. R., Alrabaiah, H., Kumam, P., Mousa, A. A. A., et al. (2022). A study of triple-mass diffusion species and energy transfer in Carreau-Yasuda material influenced by activation energy and heat source. *Sci. Rep.* 12 (1), 10219–10317. doi:10.1038/s41598-022-13890-y

Song, Y. Q., Waqas, H., Al-Khaled, K., Farooq, U., Gouadria, S., Imran, M., et al. (2022). Aspects of thermal diffusivity and melting phenomenon in Carreau nanofluid flow confined by nonlinear stretching cylinder with convective Marangoni boundary constraints. *Math. Comput. Simul.* 195, 138–150. doi:10.1016/j.matcom.2022.01.001

Wang, F., Nazir, U., Sohail, M., El-Zahar, E. R., Park, C., and Thounthong, P. (2022). A Galerkin strategy for tri-hybridized mixture in ethylene glycol comprising variable diffusion and thermal conductivity using non-Fourier's theory. *Nanotechnol. Rev.* 11 (1), 834–845. doi:10.1515/ntrev-2022-0050

Nomenclature

Z, Y, X space coordinates
B_0 magnitude of magnetic field
B_e Hall parameter
G gravitational acceleration
T_∞ ambient temperature
n power law index number
λ mixed convection number
C_p specific heat capacitance
Ω angular velocity
μ fluidic viscosity
$\gamma F, \Theta$ dimensionless velocity and temperature
W Weissenberg number
Pr Prandtl number
H_t heat source parameter
Sc_∞ Schmidt number at infinity
Re Reynolds number
Nu Nusselt number
PDEs partial differential equations
w_2, w_1, w_3 weight functions
ψ_j shape function
$\tilde{V}$ fluid velocity vector
$\mathbf{\nabla}$ gradient operator
τ Cauchy stress tensor
B magnetic induction
V, W, U velocity components
σ electrical conductivity
B_i ion slip number
T fluid temperature
β coefficient of thermal expansion
Γ time relaxation number
ρ fluid density
K thermal conductivity
T_w wall temperature
μ_∞ ambient viscosity
ϵ very small number
Θ_γ fluidic viscosity
M magnetic parameter
Pr_∞ Prandtl number at infinity
Sc Schmidt number
γ_1 thermal relaxation number
C_f skin friction coefficient
ODEs ordinary differential equations
FEM finite element method
η independent variable
η_e, η_{e+1} stiffness elements
E electrical field vector
d/dt material derivative
J vector current density
Q heat flux vector